Proceedings of ASME Turbo Expo 2012: Power for Land, Sea and Air
ASME 2012
June 11-15, 2012, Copenhagen, Denmark

GT2012-68241

OBTAINING BIFURCATION DIAGRAMS WITH A THERMOACOUSTIC NETWORK MODEL

Giovanni Campa*

D.I.M.eG.
Politecnico di Bari
via Re David 200, 70125 Bari, Italy
Email: g.campa@poliba.it

Matthew P. Juniper

Engineering Department
University of Cambridge
Trumpington Street, Cambridge,
CB2 1PZ, United Kingdom
Email: mpj1001@cam.ac.uk

ABSTRACT

Linear techniques can predict whether the non-oscillating (steady) state of a thermoacoustic system is stable or unstable. With a sufficiently large impulse, however, a thermoacoustic system can reach a stable oscillating state even when the steady state is also stable. A nonlinear analysis is required to predict the existence of this oscillating state. Continuation methods are often used for this but they are computationally expensive.

In this paper, an acoustic network code called LOTAN is used to obtain the steady and the oscillating solutions for a horizontal Rijke tube. The heat release is modelled as a nonlinear function of the mass flow rate. Several test cases from the literature are analysed in order to investigate the effect of various nonlinear terms in the flame model. The results agree well with the literature, showing that LOTAN can be used to map the steady and oscillating solutions as a function of the control parameters. Furthermore, the nature of the bifurcation between steady and oscillating states can be predicted directly from the nonlinear terms inside the flame model.

NOMENCLATURE

A amplitude
C coefficient in Levine-Baum model
h generic function
i imaginary unit
$\Im$ imaginary part
k flame constant
m mass flow rate
p pressure
q derivative of heat release rate
Q heat release rate
r nonlinear flame model amplitude
R control parameter
$\Re$ real part
t time
T transfer matrix
u velocity
x amplitude of the fundamental mode

Greek:

α saturation ratio
ε small parameter
ζ damping coefficient
η velocity fluctuation
λ oscillation period
μ polynomial function's coefficient
ϕ phase
τ time delay
ω angular frequency

*Address all correspondence to this author.

Superscripts:

$\bar{}$ mean quantity
$'$ fluctuating quantity
$\hat{}$ complex quantity
L linear
m frequency harmonic

Subscripts:

F fold point
H Hopf point

INTRODUCTION

Combustors often suffer from thermoacoustic instabilities, which lead to large amplitude pressure and heat release oscillations. These instabilities are due to coupling between the unsteady heat release rate and the acoustic oscillations inside the combustor. Such oscillations can lead to violent vibrations within the system, with the risk of complete failure.

In the 1960's it was observed that some stable solid rockets motors would suddenly jump to a self-sustained oscillation state, when pulsed [1]. A similar problem has been observed in gas turbine combustion chambers [2] and in models of thermoacoustic systems [3–5].

Many studies were carried out on rocket engines, where the oscillations have such high amplitudes that the gas dynamics are nonlinear [6–12]. Most of these analyses considered nonlinear gas dynamics and linear combustion models. The conclusion of these studies was that nonlinear gas dynamics, even up to third order, is not able to explain triggering [13]. Nonlinear combustion was later considered [3, 14, 15]. In these papers the heat release was a quadratic or rectified (modulus sign) function of the fluctuating velocity and pressure. These studies showed that triggering could be achieved when nonlinear combustion is taken into account and different types of nonlinear models that give rise to experimentally-observed behaviour were explored.

Lean premixed combustion has been introduced in gas turbine engines in order to reduce the emission of NO_x. This, however, increases susceptibility to thermoacoustic instability, leading to increased interest in this subject [16]. The energy density is considerably less than that in a rocket engine so the thermoacoustic oscillations have lower amplitude and are usually sufficiently small that nonlinear gas dynamics can be neglected. Moreover, in gas turbines, the heat release fluctuations tend to be a function of the velocity fluctuations rather than the pressure fluctuations. This paper is restricted to linear gas dynamics and nonlinear combustion with velocity coupling because triggering seems to be particularly influenced by nonlinear combustion but not by nonlinear gas dynamics.

The main aim of this paper is to show that it is easy for network models such as LOTAN to map the bifurcation diagram as a function of a control parameter. The velocity-coupled heat release response is varied. This is one of the most influential factors that determines whether the Hopf point leads to a subcritical or a supercritical bifurcation, as well as whether there is a subsequent fold bifurcation. The bifurcation diagrams show the amplitude of limit cycles as a function of the parameters of the system. This is useful if there is a known bound on the acceptable oscillation amplitude. They also show whether the point of linear instability (the Hopf bifurcation) is supercritical or subcritical. This is an important qualitative distinction because: in a subcritical system, high amplitude oscillations appear suddenly when the flow becomes linearly unstable; in a supercritical system, the system can exhibit self-sustained oscillations even when it is linearly stable.

After a brief introduction to nonlinear flame models and bifurcation diagrams (Section 1 and 2), there is a brief explanation about how LOTAN works (Section 3). In Section 4 several nonlinear flame models from the literature are then examined in order to test different types of nonlinearities. The obtained results from LOTAN are compared with those from the literature in order to assess the ability of LOTAN to map the bifurcation diagrams. All these analyses are applied to a simple horizontal Rijke tube. This is sufficient here because this work is concerned with the heat release model rather than the acoustic network. The same qualitative behaviour is expected in more complex acoustic networks.

1 Non-Linear Analysis

Linear models are not able to predict triggering instabilities and limit cycle amplitudes. In order to get this kind of information, nonlinearities must be introduced into the model and the analysis. In Fig. 1 two diagrams with the same control parameter R are shown. The variable on the vertical axis is the steady state amplitude of the system, which is often the peak-to-peak amplitude of the oscillations. At low values of R there is a solution with zero amplitude, which is known as the stable solution at zero (solid line in the figure). When R reaches R_H, this solution becomes unstable. This point is known as a Hopf bifurcation point. For R greater than R_H, the solution at zero amplitude is unstable (dashed line) and the system starts to oscillate and eventually reaches the steady state amplitude (solid line at non-zero amplitudes), which is the limit cycle or the stable periodic solution.

The nonlinear behaviour around the Hopf bifurcation point determines two different types of bifurcation. The first type is the supercritical bifurcation (Fig. 1a) and it is characterized by a gradually increase of the amplitude as $R > R_H$. For $R < R_H$ all perturbations imposed on the system tend to decay to zero, whereas for $R > R_H$ all the perturbations tend to reach a new

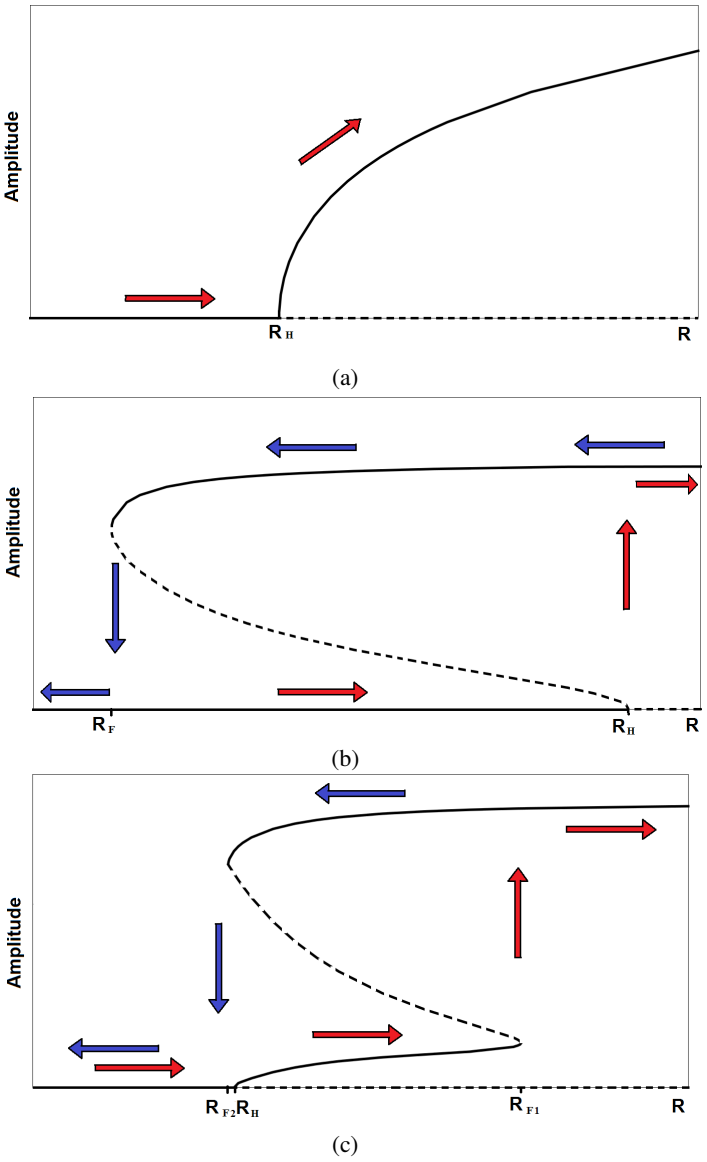

FIGURE 1. Steady state oscillation amplitude as a function of R for (a) a supercritical bifurcation and (b-c) a subcritical bifurcation. As the control parameter R is increased, the system follows the red arrow path. As it is decreased, the system follows the blue arrow path.

stable periodic solution, which is a limit cycle equilibrium. As the control parameter R is increased, the system follows the red arrow path. As it is decreased, the system follows the blue arrow path. The second type is the subcritical bifurcation (Fig. 1b) and it is characterized by a sudden increase of the steady state amplitude as R increases through R_H, reaching the limit cycle equilibrium at higher amplitudes (red arrows path). Decreasing the control parameter R, the perturbations imposed on the system reach a stable periodic solution until $R = R_F$ with $R_F < R_H$, where R_F is referred to the fold point. As R decreases through R_F all perturbations decay to zero, as shown by the blue arrow path in Fig. 1b. The dashed line in Fig. 1b, located between R_F e R_H, is known as the unstable periodic solution [17]. Fig. 1c shows a particular type of subcritical bifurcation, since it is composed of an initial supercritical bifurcation with two fold points which determine the subcritical behaviour of the bifurcation diagram. The arrows in the figure explain how the system answers to the perturbations imposed on it.

Bifurcation diagrams can be obtained by systematic variation of parameters and tracking direct time integration [18, 19], even if this method is computationally expensive. The basins of attraction of the limit cycle do not depend on the initial state. The initial state determines which basin of attraction the state is in.

Another method for obtaining the bifurcation diagram is numerical continuation [15, 20, 21]. This approach is based on the iterative solution of a set of parameterized nonlinear equations given an initial guess. The diagram is tracked varying a parameter and including the solutions which satisfy the set of equations for a given state of the system. The advantages are that an unstable limit cycle can be computed and that it is very efficient in obtaining the dependance of the solution from the control parameter compared to the other methods. The disadvantage is that it takes a long time to map the bifurcation diagram and becomes too computationally expensive for more than around 100 degrees of freedom. Thanks to improvements in the method and in the parallel computing, continuation methods are likely to become important tools in nonlinear analysis of thermoacoustics.

DDE-BIFTOOL is a software based on the numerical continuation methods for delay systems [22, 23]. The steady state of the system is evaluated iteratively through the Newton-Raphson scheme and the steady state solution is used for tracking the bifurcation diagram as the control parameter varies. This has been used by Juniper [24] and Subramanian [25].

In this paper the bifurcation diagrams are obtained by means of an acoustic network model called LOTAN. This is similar to the Flame Describing Function approach described in Noiray [26] and some of Dowling's earlier papers [27].

2 Weakly Nonlinear Analysis

The appropriate analysis for determining the nature of a Hopf bifurcation point is a weakly nonlinear analysis. This has been performed before on thermoacoustic systems [6] and makes similar assumptions to the time averaging approach in many of Culick's papers. This paper differs from others due to the Maclaurin expansion (2) and because the weakly nonlinear analysis is performed on a generic governing equation for fluctuations around the steady state in a single mode thermoacoustic system:

$$\ddot{x} + x + \zeta\dot{x} + Q(x(t-\tau)) = 0. \quad (1)$$

The variable x can be identified with the amplitude of the fundamental mode of the velocity fluctuation, η, in a simple Rijke tube model [4, 24] or with η in Ref. [8]. In line with Refs. [4, 24] the damping coefficient, ζ, appears explicitly and the heat release is velocity-coupled with a time delay τ.

One of two assumptions must be made: (1) that the time delay, τ, is small compared with the oscillation period, λ, or (2) that x is periodic in t. The first of these is chosen here because it is less restrictive, so $Q(x(t-\tau)) \approx Q(x-\tau\dot{x})$. In a moment a weakly nonlinear analysis around the Hopf bifurcation point will be performed, at which oscillations in Q are small. In this case it is valid to take the Maclaurin expansion of Q:

$$Q(x(t-\tau)) \approx Q_1 \times (x-\tau\dot{x}) + Q_2 \times (x-\tau\dot{x})^2 + Q_3 \times (x-\tau\dot{x})^3 + \ldots, \tag{2}$$

where $q_1 \equiv Q'(0)$, $q_2 \equiv Q''(0)/2!$ and $q_3 \equiv Q'''(0)/3!$. For the weakly nonlinear analysis, this expansion is more general than assuming that Q is a specified function of η, as in Refs. [3, 6, 8, 10–13, 15, 28, 29]. In this paper, Q will be expanded only to third order because this is the lowest order that determines the behaviour around the Hopf bifurcation point. Eq.(2) is substituted into Eq.(1), which is re-arranged to give:

$$\ddot{x} + (1+q_1)x + (\zeta - \tau q_1)\dot{x} + q_2(x-\tau\dot{x})^2 + q_3(x-\tau\dot{x})^3 = 0. \tag{3}$$

The first two terms are those of a harmonic oscillator with frequency $(1+q_1)^{1/2}$. (The shift in frequency due to heat release was noted by Rayleigh [30] pp. 226-227.) The third term represents the first order competition between heat release and damping. Around the Hopf bifurcation point they nearly cancel so this term is small. The final two terms are nonlinear and are small around the Hopf bifurcation because the amplitude of x is small. Eq.(3) can therefore be put into the form:

$$\ddot{x} + (1+Q)x + \varepsilon h(x,\dot{x}) = 0, \tag{4}$$

where ε is a small parameter. It is then susceptible to a two-timing analysis [17].

A fast time, λ, and a slow time, T, are defined such that $\lambda = t$ and $T = \varepsilon t$. These variables, T and λ, are treated as if they are independent. The variable x is then expressed as a function of λ, T, and ε. The variables $\dot{x}$ and $\ddot{x}$ are evaluated using the chain rule:

$$x(\lambda,T,\varepsilon) = x_0(\lambda,T) + \varepsilon x_1(\lambda,T) + \mathscr{O}(\varepsilon^2) \tag{5}$$

$$\dot{x} = \frac{\partial x_0}{\partial \lambda} + \varepsilon\left(\frac{\partial x_1}{\partial \lambda} + \frac{\partial x_0}{\partial T}\right) + \mathscr{O}(\varepsilon^2) \tag{6}$$

$$\ddot{x} = \frac{\partial^2 x_0}{\partial \lambda^2} + \varepsilon\left(\frac{\partial^2 x_1}{\partial \lambda^2} + 2\frac{\partial^2 x_0}{\partial \lambda \partial T}\right) + \mathscr{O}(\varepsilon^2). \tag{7}$$

Eq.(5 – 7) are substituted into Eq.(3) and equated at different orders of ε. At $\mathscr{O}(\varepsilon^0)$ and $\mathscr{O}(\varepsilon^1)$ respectively:

$$\frac{\partial^2 x_0}{\partial \lambda^2} + (1+q_1)x_0 = 0, \tag{8}$$

$$\frac{\partial x_1}{\partial \lambda^2} + 2\frac{\partial^2 x_0}{\partial T \partial \lambda} + (1+q_1)x_1 + (\zeta - \tau q_1)\frac{\partial x_0}{\partial \lambda} + q_2\left(x_0 - \tau\frac{\partial x_0}{\partial \lambda}\right)^2 + q_3\left(x_0 - \tau\frac{\partial x_0}{\partial \lambda}\right)^3 = 0. \tag{9}$$

If variations of x_0 in the slow timescale, T, are frozen then Eq.(8) collapses to an O.D.E. with solution

$$x_0 = r\cos(\omega\lambda + \phi), \tag{10}$$

where $\omega^2 = (1+q_1)$ and r and ϕ are functions of the slow time, T. Eq.(10) is substituted into Eq.(9), which is re-arranged to give an inhomogeneous O.D.E. for x_1:

$$\frac{d x_1}{d\lambda^2} + \omega^2 x_1 = \left[2\omega r\phi' - q_3\tfrac{3(1+\tau^2\omega^2)}{4}r^3\right]\cos(\omega\lambda+\phi) + \left[2\omega r' + (\zeta - \tau q_1)\omega r - q_3\tfrac{3\tau\omega(1+\tau^2\omega^2)}{4}r^3\right]\sin(\omega\lambda+\phi) + \text{terms in } \cos n(\omega\lambda+\phi) \text{ and } \sin n(\omega\lambda+\phi) \text{ where } n \neq 1. \tag{11}$$

To avoid secular terms, the expressions in square brackets in Eq.(11) must be zero. This leads to an expression for the evolution of the amplitude, r, and phase, ϕ, on the slow timescale, T, for $r \neq 0$:

$$\frac{dr}{dT} = \frac{(\tau q_1 - \zeta)}{2}r + \frac{3\tau(1+\tau^2\omega^2)}{8}q_3 r^3 \tag{12}$$

$$\frac{d\phi}{dT} = \frac{3(1+\tau^2\omega^2)}{8\omega}q_3 r^2 \tag{13}$$

The first term on the RHS of Eq.(12) represents linear driving if $\tau q_1 > \zeta$ and the second term represents cubic saturation if q_3 is negative or cubic enhancement if q_3 is positive. There is a periodic solution if $dr/dT = 0$, which occurs when

$$r = \pm\left(\frac{4(\zeta - \tau q_1)}{3q_3\tau(1+\tau^2\omega^2)}\right)^{1/2}. \tag{14}$$

Assuming that q_1 is positive, this gives two types of solution, depending on whether q_3 is positive or negative, as shown in Fig. 2.

The same result can be derived with a time-averaging approach. This shows that cubic terms are required in order to predict whether a bifurcation is supercritical or subcritical.

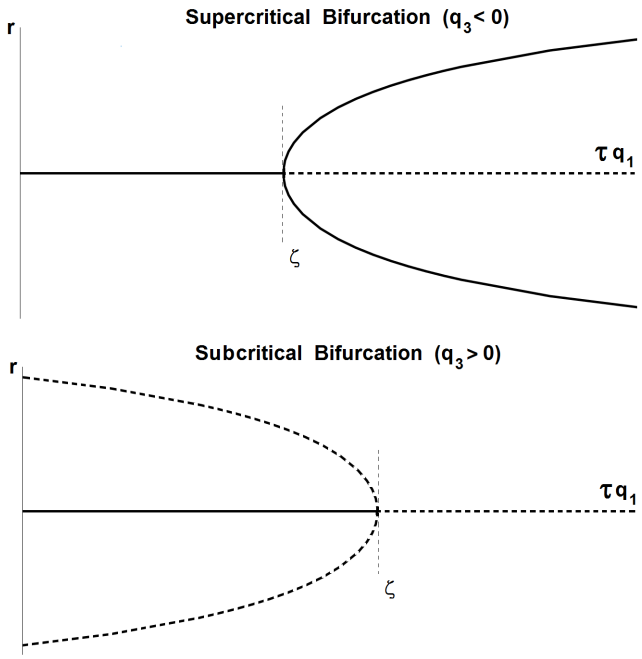

FIGURE 2. Bifurcation diagrams around the Hopf point predicted from the weakly-nonlinear analysis. Solid lines are stable solutions. Dashed lines are unstable solutions. The type of Hopf bifurcation depends on the sign of q_3 in Eq.(14). q_3 is the third derivative of $q(x)$ in the Maclaurin series Eq.(2).

3 LOTAN's Approach

LOTAN is an acoustic network model which uses linear theory to predict the combustion oscillations in LPP combustors [31–33]. It is possible to obtain the frequencies of the resonant modes, their stability, and their modeshapes. Introducing nonlinear flame models, it is possible to predict the limit cycle amplitudes both in the frequency and in the time domain.

The model assume a perfect gas with temperature written in terms of pressure and density. The flow is assumed to be composed of a steady axial mean flow and a small perturbation. The mean flow and the perturbations can be assumed to be one-dimensional. The model is formulated in terms of a network of modules describing the features of the geometry, where straight ducts are joined by other modules. Due to the modular form, other components could easily be added to the model, such as area changes and combustion zones. For the straight ducts modules, wave propagation is used to relate the perturbations at one end of the duct to those at the other. The rest of the modules are assumed to be acoustically compact. Quasi-steady conservation laws for mass, momentum and energy are used to find the perturbations. At a combustion zone, the unsteady heat release is related to the flow disturbances by a flame transfer function. Acoustic boundary conditions are imposed at inlet and outlet of the geometry. In order to find the resonant modes of the system, an initial value for ω is guessed and the perturbations are calculated, starting at the inlet and stepping through the modules to the outlet. Usually this solution will not match the outlet boundary condition, so ω is iterated to satisfy this constraint. The frequency is $\Re(\omega)/(2\pi)$, and the growth rate of the oscillations is defined as $-\Im(\omega)$. If the growth rate is negative, the mode is linearly stable, whereas if the growth rate is positive, the mode is unstable and the oscillations grow in amplitude until nonlinear effects become important and a limit cycle is achieved.

Combustion is assumed to take place in a single zone, which is acoustically compact in the axial direction. The flame model relates the heat release fluctuations Q' to the unsteady flow at previous times. Eq.(15) shows an example of a simple saturation flame model:

$$Q'(t) = \begin{cases} Q'(t) & for \mid Q'(t) \mid \leq \alpha\overline{Q}, \\ \alpha\overline{Q} sign(Q'(t)) & for \mid Q'(t) \mid > \alpha\overline{Q}, \end{cases} \tag{15}$$

where α is the saturation ratio, the prime denotes a perturbation and the overbar a mean value, so that $Q(t) = \overline{Q} + Q'(t)$. In the frequency domain the perturbed quantities are regarded as complex functions of time:

$$m'(t) = \Re(\widehat{m}e^{i\omega t}). \tag{16}$$

Also heat release can be represented as a complex function:

$$Q'(t) = \Re(\widehat{Q}e^{i\omega t}). \tag{17}$$

The (linear) flame transfer function used in linear-mode calculations is defined by:

$$T^L_{flame}(\omega) = \frac{\widehat{Q}/\overline{Q}}{\widehat{m}/\overline{m}} = -ke^{-i\omega\tau}, \tag{18}$$

where τ is the time delay and k is the flame constant. In the case of a flame, k represents a dimensionless constant of proportionality between the heat release and the mass flow.

For finite disturbances, $Q'(t)$ may not be harmonic. If it is still periodic, it can be described by a Fourier series:

$$Q'(t) = \Re\left(\sum_{m=0}^{\infty} \widehat{Q}e^{im\omega t}\right). \tag{19}$$

In frequency domain limit cycle calculations, higher harmonics are neglected such that $\widehat{Q} = \widehat{Q}^{(1)}$. It is acceptable to neglect these

harmonics in heat release because, if the velocity fluctuation is harmonic, the change in acoustic energy due to these harmonics integrates to zero over a cycle. In so doing, a nonlinear flame transfer function is defined as a function of frequency and amplitude $A = \mid \widehat{m} \mid / \overline{m}$. The first Fourier coefficient is equal to:

$$\widehat{Q}^{(1)} = \frac{\omega}{\pi} \int_0^{2\pi/\omega} Q'(t) e^{i\omega t} dt. \tag{20}$$

Using Eq.(15) and Eq.(16), depending on the flame model, the nonlinear flame transfer function NFTF is obtained and expressed as a multiple of the linear transfer function:

$$NFTF = \frac{T_{flame}(\omega, A)}{T^L_{flame}(\omega)} = \frac{\widehat{Q}^{(1)}}{\widehat{Q}^L}, \tag{21}$$

with $\widehat{Q}^L$ being the value from the linearised flame model. The dependance of the flame transfer function on the amplitude A is investigated in order to detect the limit cycle amplitudes and to build the bifurcation diagram. LOTAN first tries to find a linear mode for the nonlinear flame model, such as Eq.(15), and then tries to reach the limit cycle in steps. At first, stepping is in the amplitude factor, which is equivalent to increasing the amplitude A of the perturbations. When the growth rate starts to decrease, stepping is transferred to the growth rate, until this is zero. At zero growth rate, the limit cycle solution r is found. It is also possible to start from an initial guess for the amplitude, rather than from zero. Further details about how the acoustic network code works and how the amplitude of the limit cycle is detected can be found in the literature [31–33].

4 Results

The behaviours of various heat release models from the literature have been compared with the corresponding behaviours obtained using LOTAN. The configuration is a simple Rijke tube with the hot wire placed at one quarter of the tube length. The temperature increases from 300 K to 700 K across the combustion zone. The time delay is not varied in this study and is fixed at $\tau = 0.02\ s$. This study isolates the amplitude dependance of the heat release and not the amplitude dependance of the time delay. Open-end inlet and outlet boundary conditions, $p' = 0$, are considered. For all cases, the control parameter for mapping the bifurcation diagram is the flame constant.

First, the saturation flame model introduced by Dowling [34] has been analysed. In this model the amplitude of heat release fluctuations increases linearly with the amplitude of the mass flux fluctuations for low amplitudes and then saturates to a constant value at high amplitudes. The bifurcation diagram has a zero fixed point, followed by a sudden jump to the stable periodic solution. This Hopf bifurcation is neither supercritical nor subcritical (it is degenerate). This is because the model switches discontinuously from linear behaviour to saturated behaviour.

Next the work by Ananthkrishnan et al. [35] has been taken as reference. This nonlinear flame model is a polynomial function of the mass flow rate. Only the influence of the odd-powered polynomial terms are examined because, although even-powered polynomial terms are physically admissible, their contribution to the acoustic energy integrates to zero over a cycle. Eq. (22) represents the nonlinear flame model with a third-powered term:

$$\frac{Q'}{\overline{Q}} = -k\left[\mu_2 \left(\frac{m'}{\overline{m}}\right)^3 + \mu_0 \frac{m'}{\overline{m}}\right]. \tag{22}$$

The position of the Hopf point is determined by the linear term (see section 2). If this is zero, the Hopf point occurs where the heat release parameter is at zero. The flame model is a cubic curve without saturation, Fig.3a. The nonlinear flame transfer function (NFTF) is a parabola with positive curvature and the intersection with the vertical axis depends on μ_0, Fig.3b. In this case $\mu_2 = 1$ and $\mu_0 = 0.2$. The NFTF is always positive for positive amplitudes A and it monotonically increases, which means that a subcritical bifurcation is expected, Fig. 4.

Beyond the Hopf point, the oscillations grow without limit because both μ_2 and μ_0 are positive. Before the Hopf point, the periodic solution is unstable for the same reason (see Fig. 2).

Next, a fifth order term is added to the previous flame model [35], Eq.(23). The coefficient μ_4 of the fifth order terms of the nonlinear flame model contributes to the bifurcation diagram at large amplitudes.

$$\frac{Q'}{\overline{Q}} = -k\left[\mu_4 \left(\frac{m'}{\overline{m}}\right)^5 + \mu_2 \left(\frac{m'}{\overline{m}}\right)^3 + \mu_0 \frac{m'}{\overline{m}}\right]. \tag{23}$$

The flame model is a fifth-powered curve without saturation, Fig. 5a. In this case $\mu_4 = 1$, $\mu_2 = -1$ and $\mu_0 = 0.3$. The NFTF is always positive and has negative curvature followed by positive curvature, Fig. 5b.

The bifurcation diagram shows a supercritical Hopf bifurcation to a stable periodic solution at small amplitudes r followed by a fold bifurcation to an unstable periodic solution at large amplitudes r, Fig. 6. This corresponds to the large increase of the FTF at high amplitudes, which occurs when $\mu_4 > 0$. The pattern shown in Fig. 6 at lower amplitudes r is similar to that shown in Fig. 3 of Ananthkrishnan and Culick [35]. There are some differences. First, the horizontal axis of Fig. 3 in Ref. [35] is the damping coefficient α_1, whereas the horizontal axis of Fig. 6 is the flame constant; the control parameter is different, but the behaviour is the same. Second, the nonlinear flame model of Anan-

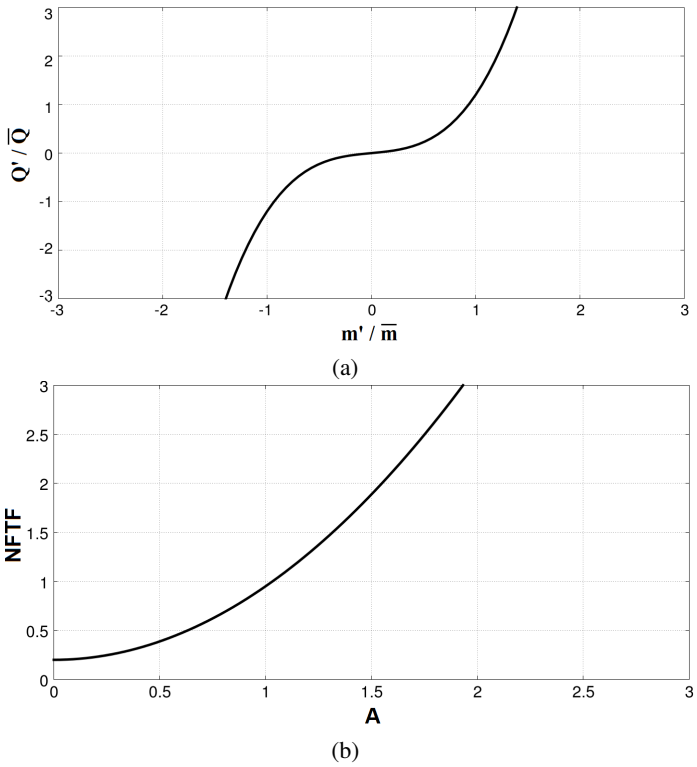

FIGURE 3. Flame Model (a) and Nonlinear Flame Transfer Function (b) for the polynomial nonlinear flame model with $\mu_2 = 1$ and $\mu_0 = 0.2$ in Eq.(22).

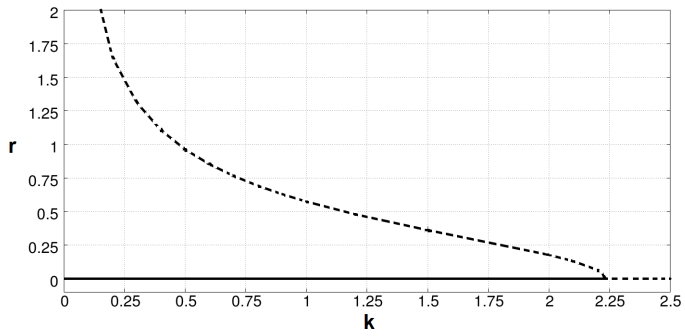

FIGURE 4. Bifurcation Diagram for the polynomial nonlinear flame model with $\mu_2 = 1$ and $\mu_0 = 0.2$ in Eq.(22).

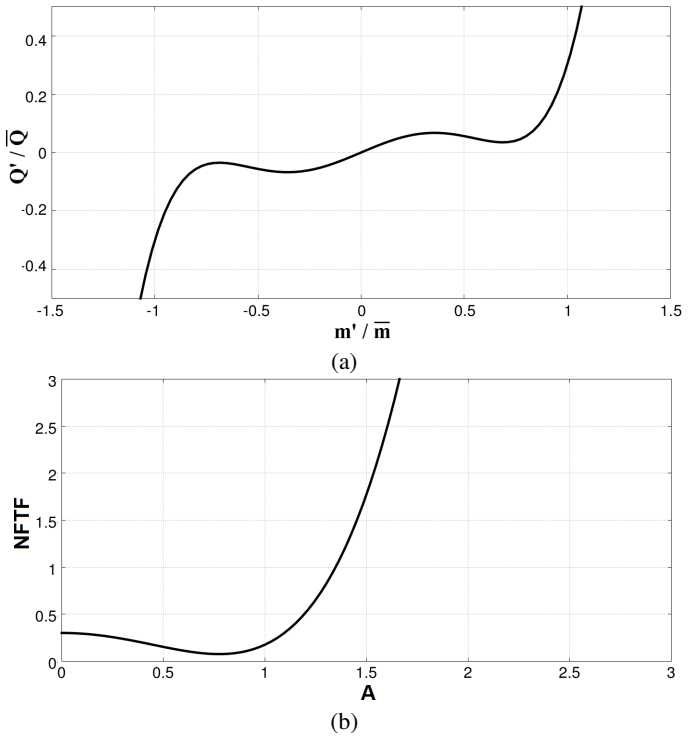

FIGURE 5. Flame Model (a) and Nonlinear Flame Transfer Function (b) for the polynomial nonlinear flame model with $\mu_4 = 1$, $\mu_2 = -1$ and $\mu_0 = 0.3$ in Eq.(23).

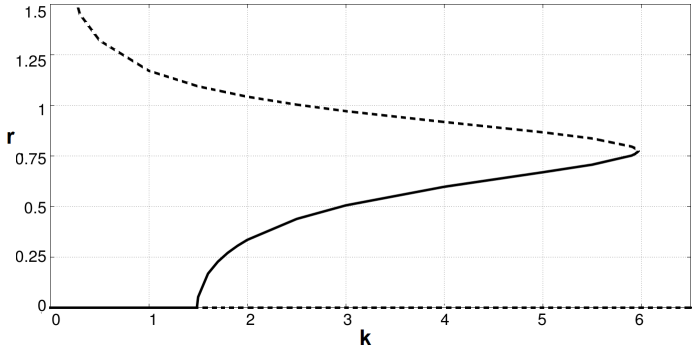

FIGURE 6. Bifurcation Diagram for the polynomial nonlinear flame model with $\mu_4 = 1$, $\mu_2 = -1$ and $\mu_0 = 0.3$ in Eq.(23).

thkrishnan and Culick contains a term, $\widehat{C}_{11}^{(2)}\dot{\eta}_2$, from the second acoustic mode, which is not present in our model.

The next flame model is similar to the previous one, Eq.(23), with different coefficient values: $\mu_4 = -1$, $\mu_2 = 1$ and $\mu_0 = 0.2$, Fig. 7a. We consider only the parts of the flame model for which the heat release perturbation has the same sign as the mass flow rate perturbation. This NFTF is always positive and has positive curvature followed by negative curvature, Fig. 7b. The bifurcation diagram shows a subcritical Hopf bifurcation to an unstable periodic solution at small amplitudes r followed by a fold bifurcation to a stable periodic solution at large amplitudes r, Fig. 8.

Wicker and Greene (1996) investigated the nonlinear combustion response inside rocket motors [3], introducing three different nonlinear flame models. The Galerkin method was used in order to investigate conditions required for triggering and the

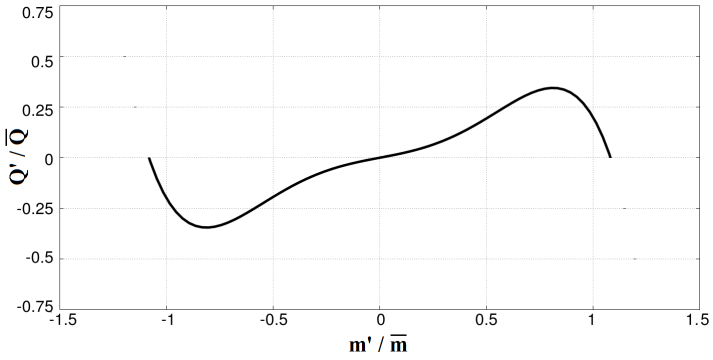

(a)

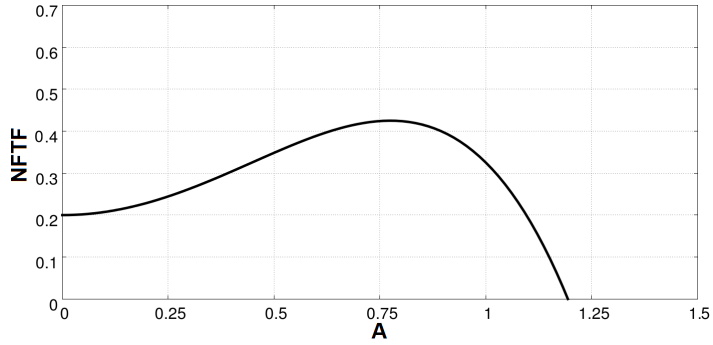

(b)

FIGURE 7. Flame Model (a) and Nonlinear Flame Transfer Function (b) for the polynomial nonlinear flame model with $\mu_4 = -1$, $\mu_2 = 1$ and $\mu_0 = 0.2$ in Eq.(23).

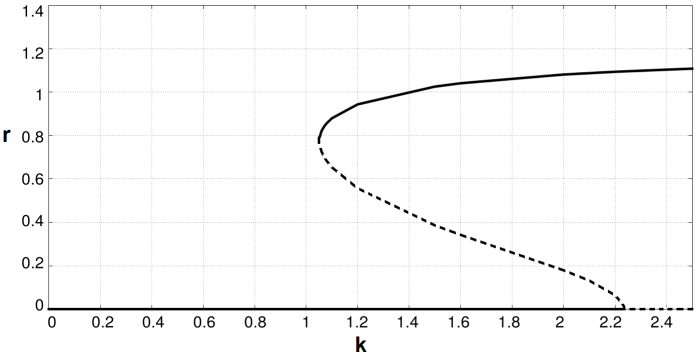

FIGURE 8. Bifurcation Diagram for the polynomial nonlinear flame model with $\mu_4 = -1$, $\mu_2 = 1$ and $\mu_0 = 0.2$ in Eq.(23).

requirements for stable initial pulses. Their flame models were:

$$\dot{Q}' \propto p'^2, u'^2, p'u', \tag{24}$$

$$\dot{Q}' \propto |u'|, |p'|; \tag{25}$$

$$\dot{Q}' \propto u'|p'|, p'|u'|. \tag{26}$$

They found that *"nonlinear combustion response proportional to quadratic functions of acoustic pressure and velocity is incapable of triggering a finite initial disturbance to a stable limit cycle"* [3]. They found that triggering to a stable limit cycle is possible if the heat release is a function of rectified (modulus sign) acoustic velocity. With LOTAN, we also find that the quadratic term in the flame model, Eq.(24), by itself, cannot determine the type of bifurcation. This is expected because the contribution of this term to the acoustic energy integrates to zero over a cycle. We also find that Eq.(25) cannot determine the type of bifurcation. This is because the gradient of the modulus sign is undefined at zero. The third flame model, Eq.(26), is very similar to that proposed by Levine and Baum [14]. Levine and Baum suggested a velocity coupling function of the form $F = f(u')u'$ with $f(u') = C^{vc}|u'|$ to model the nonlinear combustion response to the acoustic velocity. Ananthkrishnan and Culick [15] used this to obtain the bifurcation diagrams through a continuation and bifurcation software called AUTO97. Following the same approach, but using the mass flow rate instead of the acoustic velocity, the nonlinear flame model has been defined, Eq.(27). The flame model is assumed to saturate as shown in Fig. 9a and as described in Eq.(15).

$$\frac{Q'}{\overline{Q}} = -k\left[C\left|\frac{m'}{\overline{m}}\right| + C_1\right]\frac{m'}{\overline{m}}. \tag{27}$$

The flame transfer function is a straight line at small amplitudes, with the linear damping coefficient C_1 determining the intersection point of the NFTF curve on the vertical axis of Fig.9b and the sign of C determining the slope of the NFTF curve at small amplitudes, Fig. 9b. At higher amplitudes, saturation determines the shape of the transfer function, which tends to zero at high amplitudes.

In this case, the Hopf bifurcation is still undefined because the gradient of the modulus function is undefined around zero. If the modulus function is smoothed around zero, the Hopf bifurcation become subcritical and leads to an unstable limit cycle.

The Levine-Baum nonlinear flame model is not entirely satisfactory without saturation because the fluctuations reach infinite amplitude. In order to overcome this problem, Levine and Baum suggested a threshold amplitude. Ananthkrishnan and Culick [15] proposed a model similar to the Levine-Baum model for small velocity values with the addition of a quadratic term for large velocity values as correction. The resultant NFTF is a parabola, which gives a fold point with a subsequent stable periodic solution, which is absent in the diagram from the Levine-Baum model without any saturation. Burnley and Culick suggested a nonlinear flame model with zero values in a narrow range around zero [21]. The threshold problem persists, however, and the model is also non-physical.

The last analyzed flame model is a form of King's law

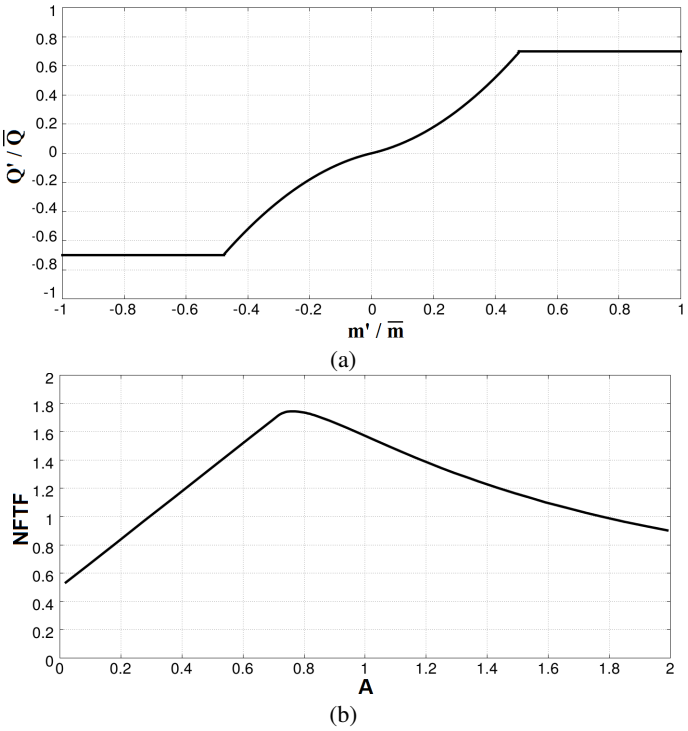

FIGURE 9. Flame Model (a) and Nonlinear Flame Transfer Function (b) for a Levine-Baum type nonlinear flame model with $C = 2$ and $C_1 = 0.5$ in Eq.(27).

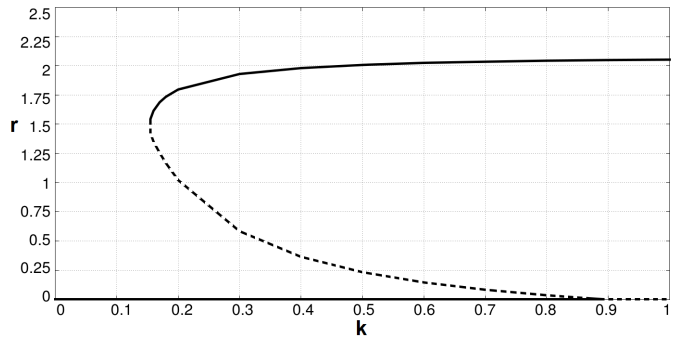

FIGURE 10. Bifurcation Diagram for a Levine-Baum type nonlinear flame model with $C = 2$ and $C_1 = 0.5$ in Eq.(27).

adapted first by Heckl [36] and then used by Balasubramanian and Sujith [4]. This model is characterized by the presence of a square root, Eq.(28), with an absolute value in order to take into account negative values. Not all the coefficients and the parameters describing the Rijke tube dimensions, present in the standard King's law [4], have been considered. Only the flame constant, k, is used as the control parameter.

$$\frac{Q'}{\overline{Q}} = -k\left(\sqrt{\left|\frac{1}{3}+\frac{m'}{\overline{m}}\right|}-\sqrt{\frac{1}{3}}\right). \tag{28}$$

A sketch of this flame model is shown in Fig. 11a. In Fig. 12

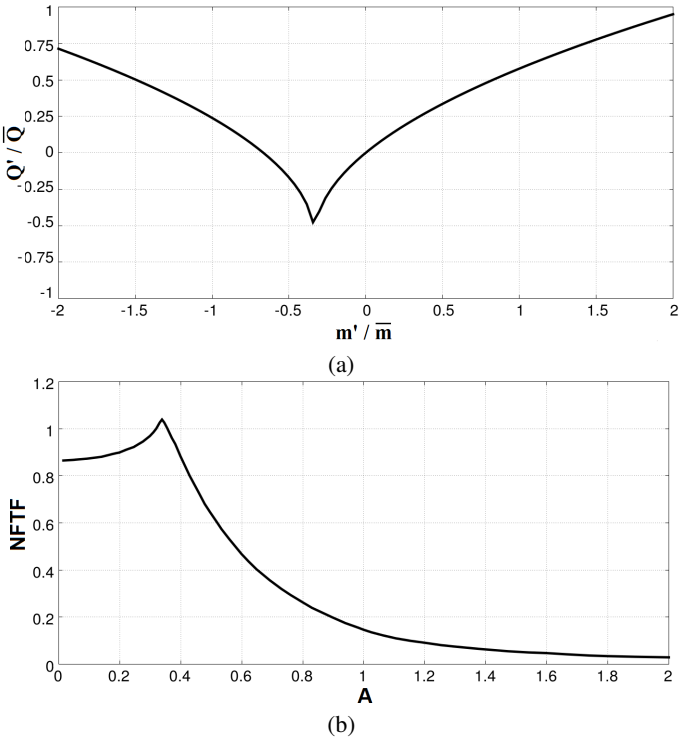

FIGURE 11. Flame model (a) and flame transfer function (b) on the form of adapted King's law in Eq.(28).

the bifurcation diagram is shown: a subcritical bifurcation is obtained. The unstable periodic solution, which is from the Hopf point to the fold point, covers a narrow range of flame constant values. The amplitude r of the stable periodic solution grows without limit as the flame constant increases. For this case, the results agree very well with those obtained by Waugh and Juniper [24, 37] using DDE-BIFTOOL. The trend is similar, but there are some obvious differences due to the different geometrical and operating parameters.

These results show that LOTAN is able to map bifurcation diagrams without any extra routines. The results agree well with those from the literature: trends are generally well caught. It is possible to determine the particular type of bifurcation directly from the flame model or from the flame transfer function. If the module of the nonlinear flame transfer function in-

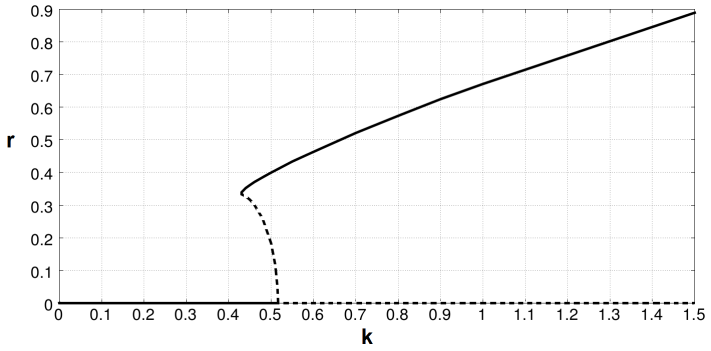

FIGURE 12. Bifurcation diagram when the flame model has the form of adapted King's law with saturation in Eq.(28).

creases from the value at zero amplitude A, a subcritical bifurcation is expected, as for the third order polynomial (Figg. 3-4), the smoothed Levine Baum type (Figg. 9-10) and the King's law type (Figg. 11-12). If the NFTF decreases from the value at zero amplitude A, a supercritical bifurcation is expected, as for the fifth order polynomial (Figg. 5-6). Generally, when the NFTF increases there is an unstable periodic solution, whereas when the NFTF decreases there is a stable periodic solution. Looking at the flame model, it is possible to predict the shape of the bifurcation diagram. If the third derivative is positive, a subcritical bifurcation is expected, otherwise a supercritical bifurcation is expected. As previously described in Section 2, a weakly nonlinear analysis determines the nature of a Hopf bifurcation point. For example, for the nonlinearity in King's law, Eq.(28), it is easy to show that $q_3 > 0$ and so the Hopf bifurcation is subcritical, Fig. 12, according to Eq.(14). The same can be done for the other flame models analysed in this paper: for the third-powered term in Eq.(22), for the fifth-powered term in Fig. 7 and for the smoothed Levine-Baum type flame model in Eq.(27) the third derivative is positive, $q_3 > 0$ and a subcritical bifurcation is obtained. For the fifth-powered term flame model in Fig. 6 the third derivative is negative, $q_3 < 0$ and a supercritical bifurcation is obtained. These results demonstrate how it is possible to predict the shape of the bifurcation diagram directly from the flame model.

5 CONCLUSIONS

In this work, the main assumption is that thermoacoustic systems should be considered within the context of nonlinear theory. The behaviour of the system is determined by the nature of the Hopf bifurcation, which can be examined both through a weakly nonlinear analysis and a continuation method. If the Hopf bifurcation is subcritical, then triggering is possible. If the Hopf bifurcation is supercritical, triggering is not certain, but may be possible.

The ratio of the linear heat release term to the linear damping term determines the position of the Hopf bifurcation point. The odd-powered terms of the flame model as a polynomial function of the mass flow rate determines the shape of the bifurcation diagram: if they are negative, the bifurcation is supercritical; if they are positive, the bifurcation is subcritical.

The main conclusion of this paper is that bifurcation diagrams can be created with LOTAN, an acoustic network model. LOTAN is simple to use and it takes little time to analyse the system in the frequency domain. Previously, LOTAN has been used to calculate the linear stability of a system, its eigenmodes and the limit cycle amplitudes r. In this paper, various nonlinear flame models from the literature have been examined and very good agreement with bifurcation diagrams from the literature has been obtained.

ACKNOWLEDGMENT

The authors would like to thank Rolls Royce PLC and Prof. Ann Dowling for permission to use LOTAN and for helpful discussions during the project.

REFERENCES

[1] Culick, F., 2006. *Unsteady Motions in Combustion Chambers for Propulsion Systems*. AGARD, AG-AVT-039.

[2] Lieuwen, T., 2002. "Experimental investigation of limit cycle oscillations in an unstable gas turbine combustor". *Journal of Propulsion and Power,* ***18***(1), pp. 61–67.

[3] Wicker, J., Greene, W., Kim, S., and Yang, V., 1996. "Triggering in longitudinal combustion instabilities in rocket motors: Nonlinear combustion response". *Journal of Propulsion and Power,* ***12***(6), pp. 1148–1158.

[4] Balasubramanian, K., and Sujith, R., 2008. "Thermoacoustic instability in a rijke tube: Nonnormality and nonlinearity". *Physics of Fluids,* ***20***, p. 044103.

[5] Balasubramanian, K., and Sujith, R., 2008. "Nonnormality and nonlinearity in combustion-acoustic interaction in diffusion flames". *Journal of Fluid Mechanics,* ***594***, pp. 29–57.

[6] Mitchell, C., Crocco, L., and Sirignano, W., 1969. "Nonlinear longitudinal instability in rocket motors with concentrated combustion". *Combustion Science and Technology,* ***1***, pp. 35–64.

[7] Chu, B.-T., 1963. "Analysis of a self-sustained thermally driven nonlinear vibration". *Physics of Fluids,* ***6***(11), pp. 1638–1644.

[8] Culick, F., 1971. "Nonlinear growth and limiting amplitude of acoustic oscillations in combustion chamber". *Combustion Science and Technology,* ***3***, pp. 1–16.

[9] Zinn, B., and Lores, M., 1972. "Application of the galerkin methods in the solution of nonlinear axial combustion instability problems in liquid rockets". *Combustion Science and Technology,* ***4***, pp. 269–278.

[10] Lores, M., and Zinn, B., 1973. "Nonlinear longitudinal combustion instability in rocket motors". *Combustion Science and Technology,* ***7***, pp. 245–256.

[11] Culick, F., 1976. "Nonlinear behavior of acoustic waves in combustion chambers - parts 1 & 2". *Acta Astronautica,* ***3***, pp. 715–734, 735–757.

[12] Paparizos, L., and Culick, F., 1989. "The two-mode approximation to nonlinear acoustics in combustion chambers i. exact solutions for second order acoustics". *Combustion Science and Technology,* ***65***(1), pp. 39–65.

[13] Yang, V., Kim, S., and Culick, F., 1990. "Triggering of longitudinal pressure oscillations in combustion chambers. i: Nonlinear gas dynamics". *Combustion Science and Technology,* ***72***(4), pp. 183–214.

[14] Baum, J., Levine, J., and Lovine, R., 1988. "Pulsed instability in rocket motors: A comparison between predictions and experiment". *Journal of Propulsion and Power,* ***4***(4), p. 308.

[15] Ananthkrishnan, N., Deo, S., and Culick, F., 2005. "Reduced-order modeling and dynamics of nonlinear acoustic waves in a combustion chamber". *Combustion Science and Technology,* ***177***, pp. 1–27.

[16] Lieuwen, T., and Yang, V., 2005. *Combustion Instabilities in Gas Turbine Engines*. AIAA.

[17] Strogatz, S., 2001. *Nonlinear Dynamics and Chaos*. Westview Press.

[18] Moeck, J., Bothien, M., Schimek, S., Lacarelle, A., and Paschereit, C., 2008. "Subcritical thermoacoustic instabilities in a premixed combustor". *14th AIAA/CEAS Aeroacoustics Conference, 2946*.

[19] Mariappan, S., and Sujith, R., 2010. "Modeling nonlinear thermoacoustic instability in an electrically heated rijke tube". *48th AIAA Aerospace Sciences Meeting Including the New Horizons Forum and Aerospace Exposition, 2010-25*.

[20] Jahnke, C., and Culick, F., 1994. "Application of dynamical systems theory to nonlinear combustion instabilities". *Journal of Propulsion and Power,* ***10***, pp. 508–517.

[21] Burnley, V., 1996. "Nonlinear Combustion Instabilities and Stochastic Sources". PhD Dissertation, California Inst. of Technology, Pasadena, USA.

[22] Engelborghs, K., and Roose, D., 2010. "Numerical computation of stability and detection of hopf bifurcations of steady state solutions of delay differential equations". *Advances in Computational Mathematics,* ***10***, pp. 271–289.

[23] Engelborghs, K., Luzyanina, T., and Roose, D., 2002. "Numerical bifurcation analysis of delay differential equations using dde-biftool". *ACM Transactions on Mathematical Software,* ***28***, pp. 1–21.

[24] Juniper, M., 2011. "Triggering in the horizontal rijke tube: Non-normality, transient growth and bypass transition". *Journal of Fluid Mechanics,* ***667***, pp. 272–308.

[25] Subramanian, P., Mariappan, S., Sujith, R., and Wahi, P., 2010. "Bifurcation analysis of thermoacoustic instability in a horizontal rijke tube". *Int. Journal of Spray and Combustion Dynamics,* ***2***(4), pp. 325–356.

[26] Noiray, N., Durox, D., Schuller, T., and Candel, S., 2008. "A unified framework for nonlinear combustion instability analysis based on the flame describing function". *Journal of Fluid Mechanics,* ***615***, pp. 139–167.

[27] Dowling, A., 1999. "A kinematic model of a ducted flame". *Journal of Fluid Mechanics,* ***394***, pp. 51–72.

[28] Awad, E., and Culick, F., 1986. "On the existence and stability of limit cycles for longitudinal acoustic modes in a combustion chamber". *Combustion Science and Technology,* ***46***(3), pp. 195–222.

[29] Yang, V., and Culick, F., 1990. "On the existence and stability of limit cycles for transverse acoustic oscillations in a cylindrical combustion chamber. 1: Standing modes". *Combustion Science and Technology,* ***72***(1), pp. 37–65.

[30] Rayleigh, W., 1896. *The Theory of Sound Vol. 2*. Dover.

[31] Stow, S., and Dowling, A., 2001. "Thermoacoustic oscillations in an annular combustor". *ASME Paper 2001-GT-0037*.

[32] Stow, S., and Dowling, A., 2004. "Low-order modelling of thermoacoustic limit cycles". *ASME paper, GT2004-54245*.

[33] Stow, S., and Dowling, A., 2008. "A time-domain network model for nonlinear termoacoustic oscillations". *ASME paper, GT2008-50770*.

[34] Dowling, A., 1997. "Nonlinear self-excited oscillations of a ducted flame". *Journal of Fluid Mechanics,* ***346***, pp. 271–290.

[35] Ananthkrishnan, N., Sudhakar, K., Sudershan, S., and Agarwal, A., 1998. "Application of secondary bifurcations to large-amplitude limit cycles in mechanical systems". *Journal of Sound and Vibration,* ***215***(1), pp. 183–188.

[36] Heckl, M., 1990. "Nonlinear acoustic effects in the rijke tube". *Acustica,* ***72***(63).

[37] Juniper, M., and Waugh, I., 2010. "Bypass transition to sustained thermoacoustic oscillations in a linearly stable rijke tube". *16th AIAA/CEAS Aeroacoustics*.